ARTICLES

Shape Control in Electrodeposited, Epitaxial CdSe Nanocrystals on (111) Gold

Irit Ruach-Nir, Yan Zhang, Ronit Popovitz-Biro, Israel Rubinstein,* and Gary Hodes*

Department of Materials and Interfaces, Weizmann Institute of Science, Rehovot 76100, Israel

Received: September 5, 2002; In Final Form: December 2, 2002

Semiconductor nanocrystals can be epitaxially electrodeposited onto single-crystal substrates. The lateral size of the nanocrystals was previously shown to be controlled mainly by the lattice mismatch between the substrate and semiconductor. Here we show that, although the lateral dimensions of the nanocrystals are only slightly dependent on the current density and temperature of deposition, the vertical dimension is strongly dependent on these parameters. This allows control of the shape and aspect ratio of the nanocrystals, from spherical at high deposition current to taller crystals with a shape between columnar and square pyramidal with rounded tops at low currents. The shape of the taller crystals is explained by considering the reduced role of kinetic factors at low current density. Cross-sectional TEM is used to image the nanoparticle shape, while photoelectrochemical spectral measurements allow approximate band gap values to be estimated for the various nanocrystals.

Introduction

Semiconductor nanocrystals are extensively studied, largely because of the three-dimensional quantum confinement which leads to an increase in the band gap and splitting of the bands into discrete levels with decrease in particle size. Thus, control over the nanoparticle size allows tailoring of the semiconductor properties.[1,2]

Although most of the effort in this field has been directed toward control of nanoparticle size and size distribution, over the past few years, the issue of particle *shape* has become an important topic of study. Variation of quantum dot shape has been shown, both theoretically [3−5] and experimentally,[6−8] to influence the energy structure of the semiconductor as well as charge relaxation dynamics.[9] Two main techniques have been used to prepare various shapes of semiconductor nanocrystals: strained heterojunction growth of one semiconductor on another, usually by MBE or CVD,[10,11] and colloidal solution growth.[12−15] Electrodeposition has been used to prepare nanostructures of defined shape by growing the electrodeposit in the pores of various porous membranes with defined pore diameter and length (templated growth).[16−18]

We have previously demonstrated epitaxial electrodeposition of CdSe nanocrystals on (111) Au films.[19,20] The epitaxy was explained by the close lattice match between CdSe and Au (based on a 2:3 ratio), while the average crystal diameter was shown to be largely determined by the degree of the mismatch strain−large strain resulting in smaller crystal size.[21] We have extended this system to include other semiconductors and substrates and found that in most cases this principle holds,[22−25] although specific chemical interaction between semiconductor and substrate is sometimes very important.[26] Although the spatial distribution of nanocrystals on the substrate could be controlled by the deposition parameters, in particular current density and temperature, (based on TEM imaging), the nanocrystal size was not found to vary strongly with these parameters.[19] TEM plan-view imaging measures lateral dimensions (although TEM contrast can provide some information on vertical dimensions for very thin samples). Using XRD to measure the height of these (0001)-oriented crystals through peak broadening, we have found that, in contrast to the lateral dimensions, the vertical dimension (height), and therefore the shape of the nanocrystals, depends strongly on the deposition parameters. Here, we show how the shape and aspect ratio of electrodeposited CdSe nanocrystals can be controlled by varying the deposition current density. We also use photoelectrochemical spectroscopy to estimate band gap values for the various CdSe samples.

Experimental Section

Electrochemical Deposition. Thick gold films (35 nm) were evaporated at 0.1 nm s^{-1} onto glass or mica slides at room temperature. The substrates were subsequently annealed in air at 250 °C for 3 (glass) or 15 h (mica). A two-electrode electrochemical cell was used to carry out the electrochemical deposition with the gold film substrate as the cathode and a Pt anode in a solution of $Cd(ClO_4)_2 \cdot 6H_2O$ (50 mM**)** and elemental Se (saturated − ≈5 mM) in DMSO. The cathode area was restricted to 1 (glass) or 2 cm^2 (mica) by RTV silicon rubber (see refs 19 and 21 for details). The plating was carried out in the constant current (galvanostatic) mode at a temperature of 90−140 °C using various current densities**.** After deposition, the substrate was dipped in hot DMSO, rinsed with water, and dried with a stream of dry air.

Characterization. A Philips CM-120 microscope operating at 120 kV was used to carry out TEM bright-field (BF) plan-

* To whom correspondence should be addressed. Fax: +972-8-9344137. E-mail: gary.hodes@weizmann.ac.il; israel.rubinstein@weizmann.ac.il.

10.1021/jp021999a CCC: $25.00
Published on Web 02/14/2003

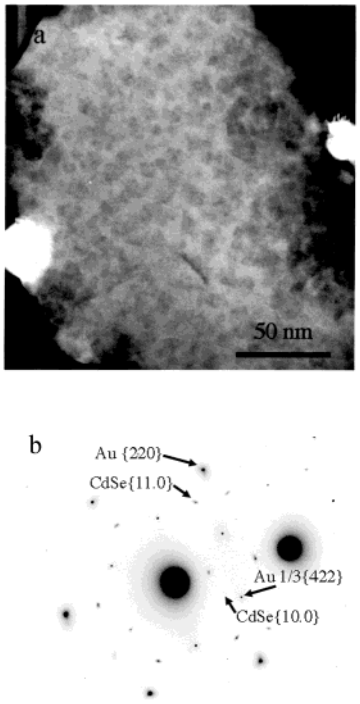

Figure 1. TEM plan view image (a) and selected area ED pattern (b) of CdSe electrodeposited on Au at 0.1 mA cm^{-2} for 15 s at 120 °C.

view and cross-section imaging and selected area electron diffraction (SAED). The CdSe/Au film was carefully separated from the glass or mica slides by dilute (∼5%) HF solution and then transferred onto copper grids for TEM plan-view measurements.

For TEM cross-section imaging the samples were embedded in epoxy resin (Embed-812, EMS) and sectioned into thin (35−50 nm) slices, using a diamond knife (Micro Star 45°) and a Leica ULTRACUT UCT Ultramicrotome. The samples were sliced perpendicular to the surface of the sample and were mounted onto polymer-coated copper grids.

X-ray diffraction (XRD) measurements were carried out with a Rigaku RU-200B Rotaflex powder diffractometer employing Cu Kα radiation at 50 kV and 150 mA**.** The coherence length (L) of the deposited crystals was estimated by the Scherrer formula, $L = k\lambda/(\beta \cos \theta)$, where λ is the wavelength of the X-ray, k is the Scherrer constant, θ is the Bragg angle of the peak, and β is the effective fwhm corrected for the instrumental broadening of the peak $\Delta 2\theta_0$ (0.317°) by $\beta = (\Delta 2\theta^2 - \Delta 2\theta_0{}^2)^{1/2}$. This gives the coherence length for cubic crystals. For spherical crystals, the crystal size is 4/3 this value.

Photoelectrochemical (PEC) measurements were carried out using monochromatized light from a xenon lamp. PEC spectroscopy was performed in an electrolyte comprising aqueous sodium selenosulfate (0.2M Se and 0.4M Na_2SO_3), in a two-electrode photoelectrochemical cell with a Pt counter electrode.

Results and Discussion

Effect of Deposition Conditions on Shape and Size. TEM plan view images of CdSe electrodeposited on Au{111} at 120 °C and current densities of 0.1 and 0.01 mA cm^{-2} are shown in Figures 1a and 2a, respectively. The same amount of charge was passed during the deposition process in both cases: 1.5 mC cm^{-2}, equivalent to a 2.5 nm thick film assuming homogeneous dispersal on the substrate and 100% current efficiency. The CdSe particles are not homogeneously distributed on the

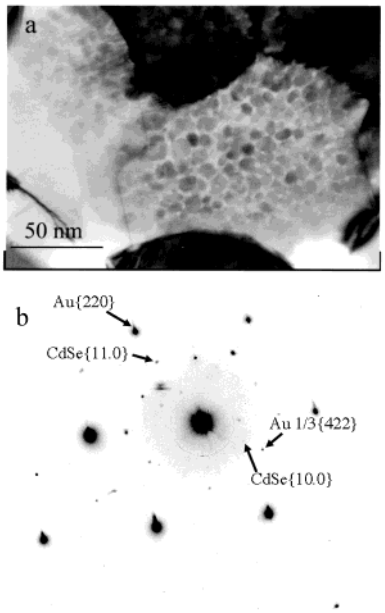

Figure 2. TEM plan view image (a) and selected area ED pattern (b) of CdSe electrodeposited on Au at 0.01 mA/cm^2 for 150 s at 120 °C.

substrate, particularly at the lower current density, but tend to form aggregates. The micrographs shown here are of areas with high densities of particles and do not represent the average thickness of the deposits.

The average size of the CdSe particles measured from these pictures is 4−5 nm for the sample deposited at 0.1 mA cm^{-2} (Figure 1a) and 5−7 nm for the sample deposited at 0.01 mA cm^{-2} (Figure 2a). There is a large difference in the contrast between the two pictures. The contrast between the CdSe particles and the gold substrate is much better for the lower current deposition (Figure 2a) than that of the higher current one (Figure 1a), and this indicates that the former particles are taller. At a deposition current of 0.4 mA cm^{-2}, the contrast was even poorer, and it was difficult to see the individual crystals.

Selected area electron diffraction (SAED) measurements of the above samples (Figures 1b and 2b) show perfect single-crystal diffraction patterns of wurtzite CdSe in epitaxial orientation with the gold (CdSe{00.1}//Au{111} and CdSe{11.0}//Au{220}).[19,20] Although the diffraction spots which correspond to {10.0}CdSe are weak, they can still be seen and indicate that the CdSe is of the wurtzite structure. Because we know from previous studies that from the second layer and up the epitaxy is no longer perfect and as the thickness increases the epitaxy is lost,[19] we can conclude that we see only a single layer of particles. This is expected also from the amount of charge passed, corresponding to an average thickness of 2.5 nm, as mentioned above.

Although TEM plan view imaging gives the lateral dimensions of the particles, XRD gives their height, as (a) only the (0002) peak of these oriented CdSe crystals is seen in XRD and (b) the (0001) planes are parallel to the (111) Au substrate surface (c-axis texture). The coherence length estimated from the XRD peak corresponds, to a first approximation, to the mean height of the crystals. The coherence length values calculated from these peaks, shown in Figure 3, are given in the figure. A small shift in the position of the peak (standard value of 25.35°) to larger angles with increasing current density is observed, mainly for the smaller crystal sizes, indicating a relief in the compressive Poisson strain (resulting from the tensile lateral mismatch strain) as the particles grow higher and further from the substrate surface.

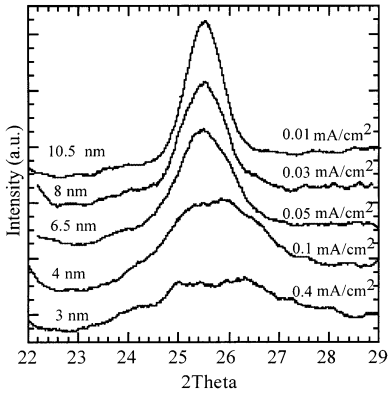

Figure 3. XRD peaks of CdSe electrodeposited on Au at 0.4, 0.1, 0.05, 0.03, and 0.01 mA cm^{-2} for 4, 15, 30, 50, and 150 s respectively at 120 °C. The coherence length is noted for each graph.

To directly image the height of the particles, cross-section TEM was carried out. Figure 4 shows a cross-section image of the sample seen in the plan view image in Figure 1. Nanoparticles with approximately spherical or hemispherical shapes are seen to grow directly on the Au substrate. The average height of the particles is 5 nm, and the average lateral diameter is 6 nm (compare with 4−5 nm from the plan view image).

Figure 5 shows a cross-section image of the low current density sample seen in plan view in Figure 2. The particle shapes vary between columnar and either conical or pyramidal, with domed tops in all cases. The heights are typically 10 nm, and the lateral diameters at the base are ∼9 nm. The lateral diameter measured from the plan view image (Figure 2) as mentioned above is 5−7 nm. Because the boundary between crystals is not clearly defined in the cross-section images, we rely more on the plan view images for the lateral dimensions and on the cross-section for the height. It should be noted, however, that for crystals with sloping sides the contrast at the middle of the crystal will be higher than at the periphery. This means that the plan image may underestimate the lateral size because the crystal boundary may not be sharp. Reverting to the plan-view micrograph of the sample electrodeposited at 0.01 mA cm^{-2} in Figure 2a, it can be seen that the cross-section is closer to a square than to a circle, although rounding is common to a certain extent. This suggests that the crystals can be best described as something between columns and square pyramids with rounding of the cross-section and with rounded tops.

If we now compare the cross-section data with the XRD results, we can refine the latter taking into account the effect of crystal shape on the measured coherence length. The heights measured from the XRD results were based on straight-edged flat crystals. For crystals with spherical symmetry (the 0.1 mA cm^{-2} and probably also the 0.4 mA cm^{-2} samples are a fair approximation to this), the coherence length should be multiplied by a factor of 4/3.[27] Taking into account the accuracy of such measurements, this is an appreciable but not a large correction. For the low current samples, we have to make a more approximate correction. For columns with rounded tops, the correction factor would be less than 4/3 and closer to unity. Calculation of the factors based on crystals with some pyramidal or conical character and rounded tops led to the conclusion that the same 4/3 factor used for spheres is, on average, reasonable. This gives actual crystal heights, estimated from the XRD data, of 4, 5, 9, 11, and 13 nm for the 0.4, 0.1, 0.05, 0.03, and 0.01 mA cm^{-2} samples, respectively. There thus appears to be a small discrepancy between the XRD and the cross-section TEM results for the 0.01 mA cm^{-2} sample (XRD = 13 nm; TEM = 10 nm).

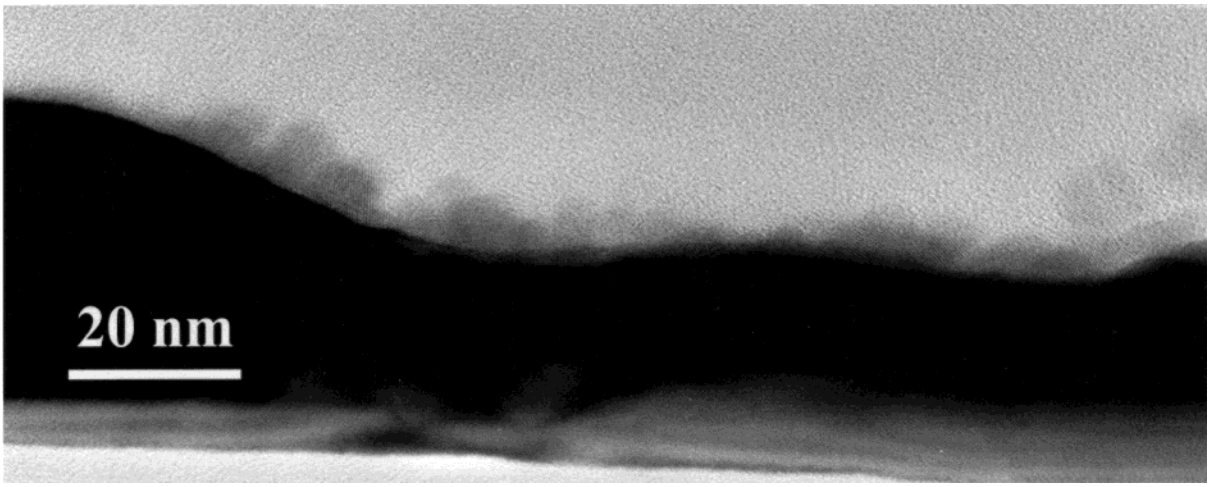

Figure 4. TEM cross section image of the sample in Figure 1.

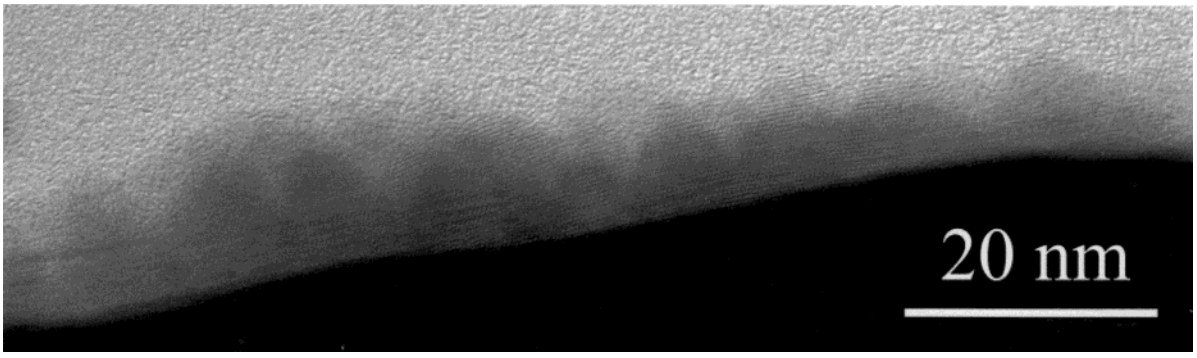

Figure 5. TEM cross section image of the sample in Figure 2.

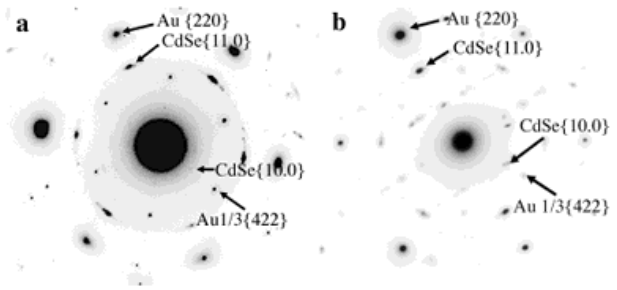

Figure 6. Selected area ED of CdSe electrodeposited on Au at 120 °C: (a) at 0.1 mA cm^{-2} for 60 s and (b) at 0.01 mA cm^{-2} for 1200 s.

There are several factors which could account for this discrepancy. XRD is known to be weighted toward the larger crystals in the distribution (above 10 nm), and this can explain some of the discrepancy. Additionally, although the boundary between the crystal base and the substrate appears to be sharp and clearly defined, from our experience in cross-section measurements, there are many cases where close observation showed that the crystal extended beyond the apparent boundary. The cross-section heights should therefore be considered as minimum values. Nonuniform strain in the crystals, if present, would cause additional XRD peak broadening. However, in this case, the XRD values would be interpreted to give a smaller crystal size rather than a larger one as measured. Therefore, considering these factors as well as the approximate nature of the XRD interpretation based on a distribution of both sizes and shapes, the disagreement between the two methods is not major. This allows us to use XRD measurements to estimate crystal heights over a larger range of experiments than would be possible using cross-section TEM imaging, which is a very time-consuming method.

Earlier experiments have shown that a second layer of crystals nucleates nonepitaxially (seen by SAED) on the first layer when deposition is carried out at 0.1 mA cm^{-2}.[19] Figure 6a shows the diffraction pattern for a film deposited at 0.1 mA cm^{-2} and 120 °C with a nominal thickness of 10 nm. The CdSe reflections are already clearly elongated, and partial ring formation occurs indicating considerable loss of epitaxy. Figure 6d in ref 21 shows even greater loss of epitaxy for a similar but thicker film ($\geqslant$ 15 nm thick). In contrast, at 0.01 mA cm^{-2}, the original crystal deposited on the substrate continues to grow as can be seen by the reasonably good epitaxy (only slight elongation of the CdSe reflections) obtained for a thicker film (nominally 20 nm thick) deposited at this lower current density (Figure 6b). In fact, even at this relatively large thickness, the substrate is not completely covered, which implies that the CdSe grows on itself in preference to the substrate. Cross-section TEM imaging of a thick layer (20 nm nominal thickness) deposited at 0.01 mA cm^{-2} further confirms this mode of growth at low deposition current (Figure 7). In this image, a large conical or pyramidal single crystal (20 nm high) of CdSe with well-defined boundaries is seen, together with aggregates of several particles with poorly defined boundaries. The epitaxy is seen to persist throughout the (rather thick) layer of particles.

Figure 8 shows the measured XRD coherence length as a function of deposition time at 0.01 mA cm^{-2}. For 100% deposition efficiency, 300 s deposition is equivalent to a 5 nm thick film (assuming a compact film). As deposition continues, the crystal height increases more or less linearly. The average lateral size, measured by TEM, increases much less with deposition time and saturates at ca. 9 nm. This saturation is a consequence of the fact that, once adjacent crystals touch, they can no longer grow in that direction (outside of coalescence of individual crystals to give a larger one).

On the basis of the influence of kinetics on crystal growth (see below), it can be expected that increase in deposition temperature should behave in the same way as decrease in deposition current density. That this is so is seen in Figure 9 which shows the increase in crystal height with increasing deposition temperature (0.01 mA cm^{-2} and 5 nm average thickness). The coherence length calculated from these peaks (after correction to the shape, multiplied by 4/3) is 4.8, 5.6, 6, 8.5, 14, and 16.5 nm for samples deposited at 90, 100, 110, 120, 130, and 140 °C, respectively.

Theoretical Reasoning for Variations in Crystal Size and Shape. We now consider the effect of deposition current on the crystal shape. At a lower current density, there is more time for the most thermodynamically stable shape, possibly pyramidal because of elimination of the high energy surface, to form. At high current density, kinetics are more likely to dictate the crystal growth. Specific factors, such as diffusion-controlled phenomena (local depletion of reactants) in the solution, will be more pronounced at higher current density.

In general, higher current density favors higher nucleation density (through higher overpotential), therefore, more nuclei for a given amount of charge and smaller crystals. This effect

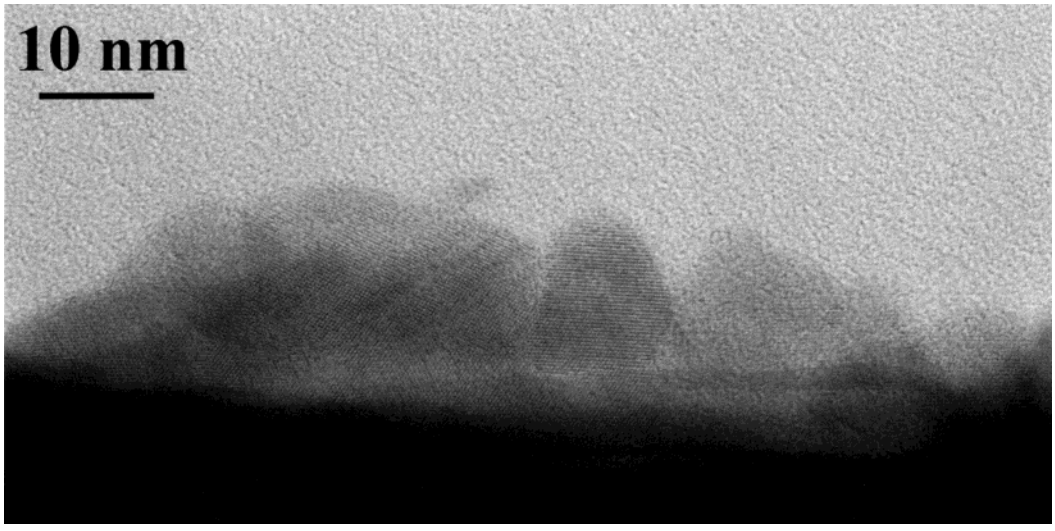

Figure 7. TEM cross-section image of a sample, nominal thickness 20 nm deposited at 0.01 mA cm^{-2} and at 120 °C.

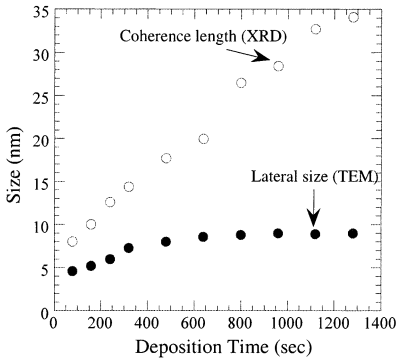

Figure 8. Coherence length measured from XRD and average lateral size measured from TEM as a function of deposition time at 0.01 mA cm^{-2}.

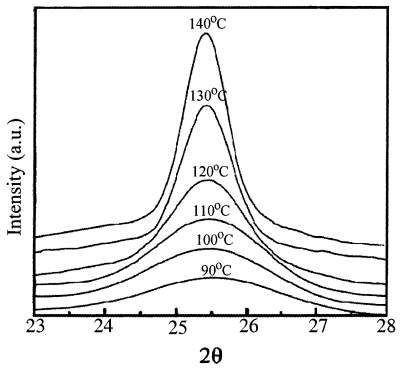

Figure 9. XRD peaks of CdSe electrodeposited at 0.01 mA cm^{-2} (nominal thickness 5 nm) at 90, 100, 110, 120, 130, and 140 °C. The coherence lengths are noted on each graph.

will be further magnified when reactant depletion is taken into account. Thus, for both these reasons, higher current densities are expected to result in smaller crystals.

Although the mechanism of crystal growth in such electrodeposition has not been unambiguously determined,[28] it does appear that growth occurs by successive deposition of the basal Cd and Se planes. Because these are probably the fastest growing planes, then, under quasiequilibrium conditions (i.e., if deposition current is low enough and/or temperature is high enough), rather than the renucleation characteristic of the high current deposits, growth can continue on the initial crystal giving a taller crystal, the shape of which depends on the energies of the various crystal planes. The rounded tops in all cases are most likely due to surface tension effects of these small crystals, whereby the surface-to-volume ratio is minimized by this configuration. A very small radius of curvature (such as in a pointed top or sharp edge) would have a very high energy, and therefore, its formation would be unfavorable.

Thus, the lateral dimensions are dictated mainly by the mismatch strain (the deposition kinetics plays some role but not a very pronounced one), while the vertical dimensions and crystal shape are dictated mainly by the deposition parameters (current density, temperature).

Band Gap Estimation by Photoelectrochemical (PEC) Spectroscopy. To obtain an estimate of the band gap of these deposits, PEC spectroscopy was employed, as the largely opaque Au substrate does not interfere as it does in regular transmission spectroscopy. PEC spectroscopy is a variant of photovoltaic photocurrent spectroscopy, where the sample is immersed in an electrolyte and the photocurrent flowing between the sample electrode and a second (nonphotoactive) electrode is measured as a function of wavelength upon irradiation of the sample. As

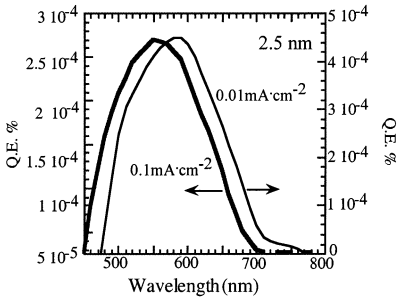

Figure 10. PEC spectra of the first layer of particles (nominal thickness 2.5 nm) electrodeposited at 0.1 and 0.01 mA cm^{-2} and at 120 °C.

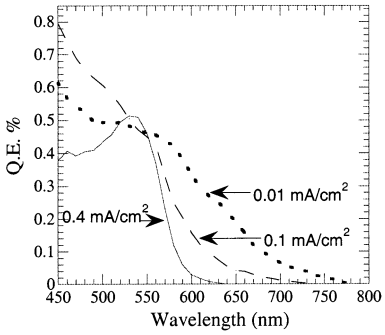

Figure 11. PEC spectra of CdSe electrodeposited at 0.4, 0.1, and 0.01 mA cm^{-2} with 10 nm nominal thickness.

in normal optical absorption spectroscopy, there is a sharp increase in the signal at the onset of light absorption (at the band gap, Eg) forming the basis for measurement of Eg. PEC is also a very sensitive technique: very small amounts of material deposited on the electrode surface can be usually detected and used to measure the band gap.[29]

Figure 10 shows such spectra of nominally 2.5 nm thick layers deposited at 0.1 and 0.01 mA cm^{-2} (the 0.4 mA cm^{-2} sample of the same nominal thickness did not give a measurable signal). The quantum efficiencies are very low because there is very little CdSe and the first layer of crystals is relatively inactive photoelectrochemically because of recombination at the CdSe/Au interface.[29] There is a clear red shift of the larger, low current samples compared to the smaller, higher current ones. Values of the band gap can be estimated from the spectra using a plot of the square of the photocurrent (or quantum efficiency) vs energy of illumination and extrapolating to zero photocurrent. This gives values of 1.81 and 1.87 eV for the larger and smaller crystals, respectively. The value of 1.87 eV for the sample deposited at 0.1 mA cm^{-2} can be compared with the value of 1.95 eV measured by the same technique for similar samples but deposited at a lower temperature (90 °C compared with the present 120 °C).[29] As seen in that study, the PEC measurements are weighted toward the larger sizes in the distribution. This is due to a combination of the longer wavelength onset of the larger crystals and, probably even more important, the higher quantum efficiency typical of larger crystals in these ultrathin samples.

Figure 11 shows PEC spectra of thicker films (10 nm nominal thickness) at three different current densities of deposition. Except for the 0.4 mA cm^{-2} (smallest crystal size) sample, which gives a band gap of ca. 2.13 eV, it is difficult to estimate band gaps from these spectra because of the prominent tailing typical of thicker films. Although some of this tailing was shown to be due to sub-bandgap response,[29] its presence makes it difficult to derive a band gap value. However, the blue-shift in the spectra as the crystal size decreases is clear.

To calculate the approximate degree of size quantization in the taller crystals, we compare the crystals with a spherical

crystal of the same volume. The ratio in volumes between a cone, pyramid, sphere, cylinder, and tetragon of equal radius (= half the pyramid/tetragon base) and height = twice the radius is 1:4/3: 2:3:4, respectively. Because in the present case, the taller crystals are both rounded at the top and appear to have some conical and columnar quality, it is a fair approximation to assume, for the purposes of estimating the degree of expected size quantization, that they can be treated as spherical. Because the size quantization in these large crystals is small in any case, any error because of this rough approximation will not affect our conclusions.

The taller crystals are then considered to behave as spherical crystals with a radius of 4−5 nm. We use the results of Murray et al. for wurtzite CdSe nanocrystals to correlate band gap and crystal size.[30] They identified the band gaps with the peaks in the optical absorption spectra. For the larger crystal sizes of interest here, which show a rather broad absorption onset, this leads to a somewhat large value of band gap (e.g., 1.80 eV for 11.5 nm; at this size, a bulk gap of 1.74 eV is expected). Re-estimation of the band gap, based on locating the gap to wavelengths slightly shorter than the absorption onset, gives values of 1.75 (11.5), 1.83 (8.3), and 1.88 eV (6.5 nm). The measured band gap value of 1.81 eV for the taller crystals thus corresponds to a spherical crystal of ca. 9.0 nm. This agrees well with the measured size of these crystals, particularly taking into account that the PEC measurements are weighted to the larger sizes.

Conclusions

Although the lateral dimensions of CdSe nanocrystals epitaxially electrodeposited onto {111} Au are determined mainly by the lattice mismatch between the CdSe and Au, the vertical dimensions and crystal shape are much more dependent on the deposition current density and deposition temperature. At relatively high current densities ($\geq$0.1 mA cm^{-2}), small (4−5 nm) roughly spherical crystals are deposited; at a low current density (0.01 mA cm^{-2}), taller ($\sim$10 nm) crystals with a shape varying between columnar and square pyramidal with rounded tops are formed. At high current densities continued deposition results in new crystals nucleating on top of the original ones, while at low current density, the crystals in contact with the Au continue to grow in height, but lateral growth is limited by neighboring crystals. The deposition temperature also plays a major role, taller crystals forming at higher temperatures. The differences in size and shape can be explained by considering crystal nucleation and the role of deposition kinetics and thermodynamics. PEC spectroscopy allowed estimation of the band gaps of the various crystals and showed the expected blue shifts with decreasing crystal size.

Acknowledgment. I.R. acknowledges support of this work by the Israel Science foundation and the Minerva Foundation, Munich. G.H. acknowledges support by the Israel Ministry of Science, Jerusalem.

References and Notes

(1) Alivisatos, A. P. *Science* **1996**, *271*, 933.
(2) Yoffe, A. D. *Adv. Phys.* **2001**, *50*, 1.
(3) Kiselev, A. A.; Kim, K. W.; Stroscio, M. A. *Phys. Rev. B* **1999**, *60*, 7748.
(4) Kim, J. N.; Wang, L. W.; Zunger, A. *Phys. Rev. B* **1998**, *57*, R9408.
(5) Li, Y. M.; Voskoboynikov, O.; Lee, C. P.; Sze, S. M.; Tretyyak, O. *J. Appl. Phys.* **2001**, *90*, 6416.
(6) Jaskolski, W.; Planelles, J.; Peris, G. *Physica E* **1999**, *4*, 176.
(7) Bissiri, M.; von Hogersthal, G. B. H.; Capizzi, M.; Frigeri, P.; Franchi, S. *Phys. Rev. B* **2001**, *6424*, art. no. 245337.
(8) Li, L. S.; Hu, J. T.; Yang, W. D.; Alivisatos, A. P. *Nano Lett.* **2001**, *1*, 349.
(9) Mohamed, M. B.; Burda, C.; El-Sayed, M. A. *Nano Lett.* **2001**, *1*, 589.
(10) Wasilewski, Z. R.; Fafard, S.; McCaffrey, J. P. *J. Cryst. Growth* **1999**, *202*, 1131.
(11) Williams, R. S.; Medeiros-Ribeiro, G.; Kamins, T. I.; Ohlberg, D. A. A. *Annu. Rev. Phys. Chem.* **2000**, *51*, 527.
(12) Manna, L.; Scher, E. C.; Alivisatos, A. P. *J. Am. Chem. Soc.* **2000**, *122*, 12700.
(13) Peng, X. G.; Manna, L.; Yang, W. D.; Wickham, J.; Scher, E.; Kadavanich, A.; Alivisatos, A. P. *Nature* **2000**, *404*, 59.
(14) Pinna, N.; Weiss, K.; Urban, J.; Pileni, M. P. *Adv. Mater.* **2001**, *13*, 261.
(15) Chen, M.; Xie, Y.; Lu, J.; Xiong, Y. J.; Zhang, S. Y.; Qian, Y. T.; Liu, X. M. *J. Mater. Chem.* **2002**, *12*, 748.
(16) Martin, C. R.; Mitchell, D. T. In *Electroanalytical Chemistry*; Bard, A. J., Rubinstein, I., Ed.; Marcell Dekker Inc.: New York, 1999; Vol. 21, p 1.
(17) Routkevitch, D.; Bigioni, T.; Moskovits, M.; Xu, J. M. *J. Phys. Chem.* **1996**, *100*, 14037.
(18) Xu, D. S.; Xu, Y. J.; Chen, D. P.; Guo, G. L.; Gui, L. L.; Tang, Y. Q. *Chem. Phys. Lett.* **2000**, *325*, 340.
(19) Golan, Y.; Margulis, L.; Rubinstein, I.; Hodes, G. *Langmuir* **1992**, *8*, 749.
(20) Golan, Y.; Margulis, L.; Hodes, G.; Rubinstein, I.; Hutchison, J. L. *Surf. Sci.* **1994**, *311*, L633.
(21) Golan, Y.; Hodes, G.; Rubinstein, I. *J. Phys. Chem.* **1996**, *100*, 2220.
(22) Golan, Y.; Ter-Ovanesyan, E.; Manassen, Y.; Margulis, L.; Hodes, G.; Rubinstein, I.; Bithell, E. G.; Hutchison, J. L. *Surf. Sci.* **1996**, *350*, 277.
(23) Golan, Y.; Hatzor, A.; Hutchison, J. L.; Rubinstein, I.; Hodes, G. *Isr. J. Chem.* **1997**, *37*, 303.
(24) Hodes, G.; Golan, Y.; Behar, D.; Zhang, Y.; Alperson, B.; Rubinstein, I. In *Nanoparticles and Nanostructured Films*; Fendler, J. H., Ed.; Wiley-VCH: Weinheim, Germany, 1998; p 1.
(25) Hodes, G.; Rubinstein, I. In *Electrochemistry of Nanoparticles*; Hodes, G., Ed.; Wiley-VCH: Weinheim, Germany, 2001; p 25.
(26) Zhang, Y.; Hodes, G.; Rubinstein, I.; Grunbaum, E.; Nayak, R.; Hutchison, J. L. *Adv. Mater.* **1999**, *11*, 1437.
(27) Guinier, A. *X-ray diffraction*; W. H. Freeman and Co.: San Francisco, 1963.
(28) Hodes, G. In *Physical Electrochemistry: Principles, Methods, and Applications*; Rubinstein, I., Ed.; Marcel Dekker Inc.: New York, 1995; p 515.
(29) Alperson, B.; Demange, H.; Rubinstein, I.; Hodes, G. *J. Phys. Chem.* **1999**, *103*, 4943.
(30) Murray, C. B.; Norris, D. J.; Bawendi, M. G. *J. Am. Chem. Soc.* **1993**, *115*, 8706.